Loughborough University

This item was submitted to Loughborough's Institutional Repository (https://dspace.lboro.ac.uk/) by the author and is made available under the following Creative Commons Licence conditions.

For the full text of this licence, please go to:
http://creativecommons.org/licenses/by-nc-nd/2.5/

MODELLING AND CONTROL OF A HIGH REDUNDANCY ACTUATOR

X. Du, R. Dixon, R. M. Goodall, and A. C. Zolotas
Control Systems Group, Department of Electronics and Electrical Engineering,
Loughborough University, Loughborough, Leicestershire, LE11 3TU, U.K.
Tel. +44 (0)1509 227015, Email: x.du@lboro.ac.uk

Abstract: The high redundancy actuation concept is a completely new approach to fault tolerance, and it is important to appreciate that it provides a transformation of the characteristics of actuators so that the actuation performance (capability) degrades slowly rather than suddenly failing, even though individual elements themselves fail. This paper aims to demonstrate the viability of the concept by showing that a highly redundant actuator, comprising a relatively large number of actuation elements, can be controlled in such a way that faults in individual elements are inherently accommodated, although some degradation in overall performance will inevitably be found. The paper introduces the notion of fault tolerant systems and the highly redundant actuator concept. Then a model for a two by two configuration with electromechanical actuation elements is derived. Two classical control approaches are then considered based on frequency domain techniques. Finally simulation results under a number of faults show the viability of the approach for fault accommodation without reconfiguration.

Keywords: fault tolerance, high redundancy, classical control

----

Email addresses: x.du@aston.ac.uk (Xinli Du),

r.dixon@lboro.ac.uk (Roger Dixon),

r.m.goodall@lboro.ac.uk (Roger M. Goodall),

a.c.zolotas@lboro.ac.uk (Argyrios Zolotas).

1. Introduction

High levels of availability and reliability are important objectives for the design of most modern engineering systems. This is particularly true in the case of safety critical applications. Hence engineers aim to produce fault tolerant designs (this applies to both the hardware/mechanisms and the control design).   The result should be fault tolerant systems, which have the capability of tolerating component malfunctions whilst still maintaining desirable and robust performance and stability properties [1]. In control terms this fault tolerance is often, but not exclusively, attained by some degree of re-configuration: i.e., detect the fault, reconfigure the system.

Practical examples of fault tolerant systems can be found in aerospace systems, e.g. Airbus fly-by-wire system [2], and Boeing 737 trailing edge flap drive system [3]. Here, low levels of functional redundancy in sensors and actuators (e.g. triplex and quadruplex) and in the control computers can be used to provide the system with the capability of fault tolerance, thereby ensuring the stability and safety of the whole system. In the above approaches, redundancy is used for fault detection and isolation (FDI) based on the continuous comparison of the system under analysis with another system characterized by the same behaviour and working in the same conditions [4]. Once a fault is detected the redundancy is then used to provide the extra control channels for the reconfiguration.

The drive-by-wire systems now have been widely used not only in aeroplane industry. The drive-by-wire systems are complex integrated systems with electronic sensors, actuators, micro-computers, information processing for single components, and engine, drive-train, suspension, and brake systems. Developed from driver-assisting systems, traditional electrically driven components,

e.g. electronic pedal and electrically driven throttle or injection, are rendered fail-safe by the mechanics [5]. The disadvantages of mechanical backup systems are that they are costly, heavy, passive safety-critical, and do not provide enough freedom to tap the potential of the electrical systems. Drive-by-wire systems without mechanical backup generate electrical commands through the driver and transfer them to computer-controlled electromechanical actuators, a scheme that is usually not fail-safe but has fault-tolerant properties [5].

A general fault-tolerant system comprising FDI and reconfiguration (R) scheme (as proposed in [1]) is illustrated in Fig. 1. The solid lines represent signal flow, and the dashed lines represent adaptation. The supervision system will reconfigure the actuator and/or sensor sets, and adapt the controller, based on the faults information collected by the FDI unit together with the inputs and outputs of the system, to accommodate the fault effects, generally though redundancies which are connected, usually in parallel. However a possible disadvantage of such approaches is the possibility of faults occurring in the FDI unit and the supervision system. One might ask the question, "Who/what monitors the monitors?".
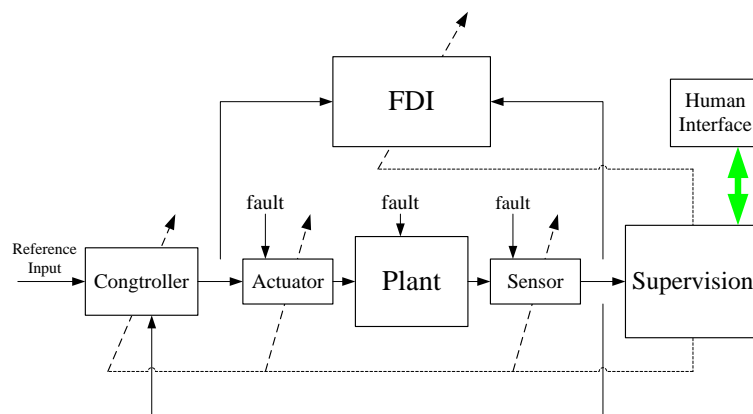

Fig. 1 Scheme of fault-tolerant control system with supervision subsystem (Patton, 1997)

This paper proposes an alternative route to fault tolerant actuation compared with the approaches discussed above. The high redundancy actuator (HRA) suggested comprises a relatively large number of actuation elements in a matrix-like structure comprising not only parallel structure but also series structure. Different from some other fault tolerant control design against actuation failures using active method, i.e. reconfiguration [6, 7, 8] and adaptive algorithms [9, 10], faults in individual actuation elements in the HRA are inherently accommodated through mechanical redundancy structure and robust control. In this design, the FDI unit may still be used for monitoring, but it is no longer strictly necessary and no reconfiguration of the controller or hardware will be needed. Instead the actuation elements work together to complete the system's objective by using the redundancy which is inherent in the structure. The HRA provides the fault tolerant ability to a component level. It combines redundancies not only in parallel, but also in series, and makes them working together under both healthy and faulty situations. When faults are injected into actuation elements, performance degradation can be expected. In practical design, it is generally unreasonable to expect a handicapped system to perform as effectively as when it is healthy. For example, the degraded performance for dynamic behaviours for an aircraft may include slower climbing rate, wider turns, slower acceleration, and other manoeuvrability [11]. For the HRA in a tracking system, the performance degradation could includes longer rise time, longer settling time, bigger overshot, but the main purpose should still be achieved, i.e. zero steady state error. If this method can be proven to work, the advantage would arise through removing the possibility of faults occurring within the FDI unit and supervision system.

Several possible structures are shown in Fig. 2. At this stage no attempt has been made to find the optimal structure for the actuators, nor have the authors attempted to identify the "best" technology for

the actuators. Instead the research has focused on modelling and control of a relatively simple (2 by 2) actuator with a view to discovering whether controlling such structures without reconfiguration is viable. Hence, the paper is structured as follows: work on modelling is presented in section 2; the control design using a classical approach is covered in section 3; then in section 4 a selection of simulation results is presented to give an indication of performance in the presence of faults alongside the fault-free case; the paper concludes in section 5, including comments on the future direction of this research.
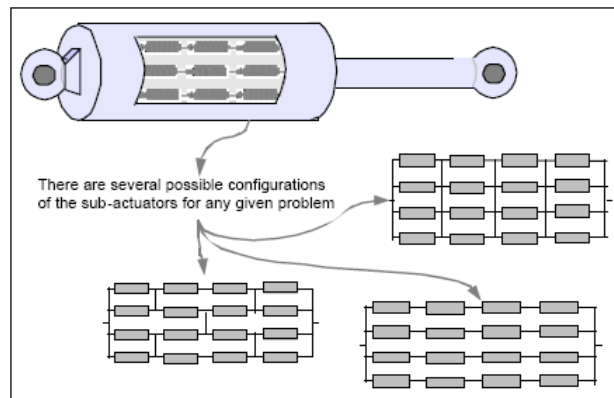

Fig. 2 Several possible configurations of the high redundancy actuator

2. Modelling

This section begins with modelling of an individual electro-mechanical actuator (the sub-actuation element inside the HRA). [An electro-mechanical actuation is chosen as the technology for this study because it is used in many industry applications, including manufacturing, process plant, railway vehicles and aerospace systems.] Next, four fault models which can affect electro-mechanical actuator will be introduced. Finally, in section 2.3, a model of a four elements two-by-two actuator will be constructed.

2.1 Modelling of individual actuator

The electro-mechanical actuator can be considered as having two parts. One is the D.C. motor, which generates the torque, and the other is the mechanical structure (screw and nut), which translates the torque generated by the motor to the load. A schematic representation of the actuator with a load is given in Fig 3, and the free body diagram is shown in Fig. 4.
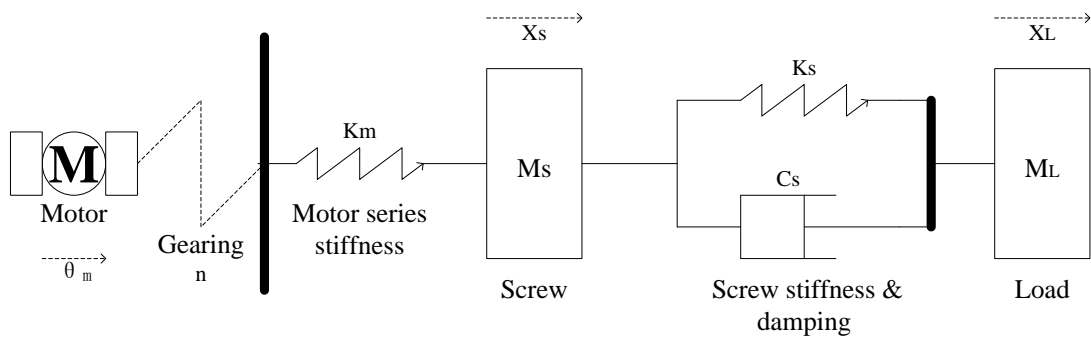
Fig. 3 Equivalent model of individual electro-mechanical actuator
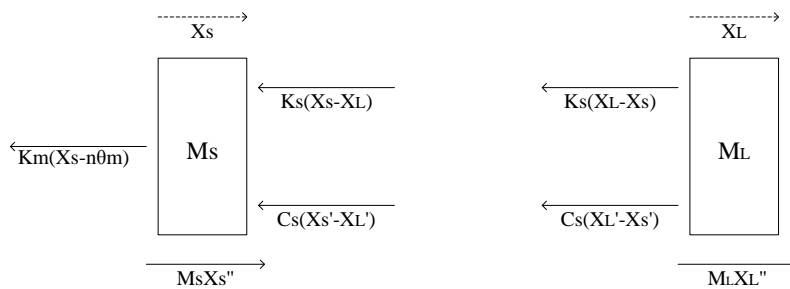
Fig. 4 Free body diagram of individual electro-mechanical actuator

On the mechanical structure, θ_m is the angular rotation of the motor shaft, n is the screw pitch, X_m and X_L are positions of the screw and the end-of-actuator (load) respectively. Although the screw and nut mechanism will normally be very stiff, it does possess finite stiffness and damping so these are included in the model. K_m represents the motor stiffness, K_s and C_s are the screw stiffness and

damping respectively. M_s and M_L are the masses of the screw and the load.

From the free body diagram, it's straightforward to obtain the differential equations:

$$\begin{cases} M_s X_s'' + K_m(X_s - n\theta_m) + K_s(X_s - X_L) + C_s(X_s' - X_L') = 0 \\ M_L X_L'' + K_s(X_L - X_s) + C_s(X_L' - X_s') = 0 \end{cases} \quad (2.1)$$

Within the D.C. servo motor, an electrical torque t_e is generated because of the electromagnetic induction. The field flux is assumed constant so that it is proportional to the armature current i_a, while it also induces a back e.m.f., which is directly proportional to the speed $\dot{\theta}_m$. Hence $t_e = K_t i_a$ and $e_r = K_e \dot{\theta}_m$, where K_e is the voltage constant depending on the number of armature turns and K_t is the torque constant which usually takes the same value as the voltage constant. The generated electromagnetic torque will be balanced by the load torque t_l, the inertial torque t_a, and the damping torque t_d, i.e. $t_e = t_l + t_a + t_d$, where $t_a = J_m \ddot{\theta}_m$, $t_d = C_m \dot{\theta}_m$, and $t_l = K_m(\theta_m n - x_m)n$ which is introduced from the load. J_m accounts for motor inertia and C_m accounts for the damping coefficient. The applied voltage relationship is given in the following equations, where R_{arm} is the resistance and L_{arm} is the inductance of the windings:

$$\begin{cases} K_t i_a - K_m(\theta_m n - X_m)n - J_m \dot{\omega}_r - C_m \omega_r = 0 \\ v_a - R_{arm} i_a - L_{arm} \dot{i}_a - K_e \dot{\theta}_m = 0 \end{cases} \quad (2.2)$$

Combining the electrical (2.2) with the mechanical (2.1) equations, a linear model can be developed in MATLAB/Simulink as presented in Fig 5.
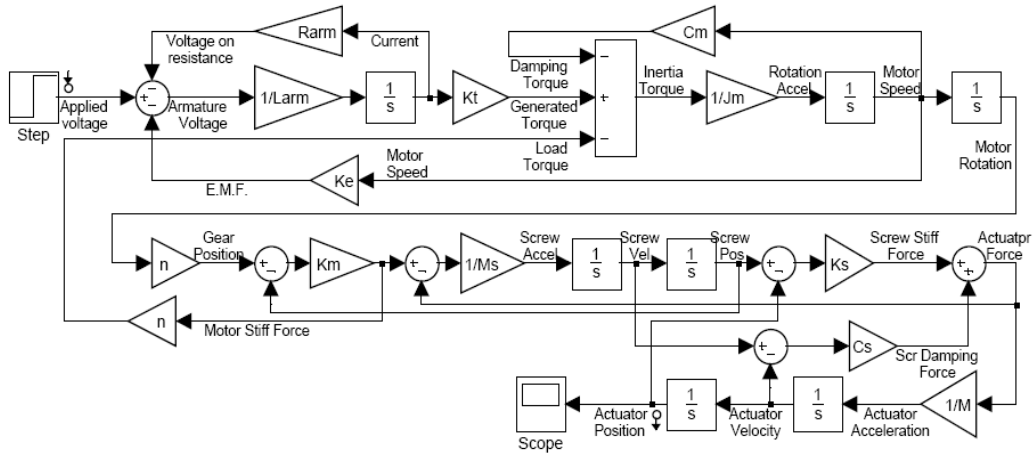
Fig. 5 Linear model of individual electro-mechanical actuator

At the output of the motor model, motor rotation is given. It is transformed by a gearing factor which provides a linear motion to the screw. The output of the actuator is a force and this force is generated by compression of the screw as the motor rotates. The actuator (and load) velocity and position are obtained based on Newton's second law, and they are fed back to the actuator model to calculate the output force.

The Simulink model is used in the time domain simulation and allows fault injection. However, to facilitate control design (in MATLAB), it is also possible to obtain the linear model in the state-space form: $\dot{x} = Ax + Bu, y = Cx$.

The state vector is chosen as $x = \begin{bmatrix} i_a & \dot{\theta}_m & \theta_m & \dot{X}_m & X_m & \dot{X}_L & X_L \end{bmatrix}^T$, and the input u and output y are chosen as $u = v_a$, $y = X_L$, where v_a is the applied voltage. The state transition, input and observation matrices for the model are:

$$A = \begin{bmatrix} -\dfrac{R_{arm}}{L_{arm}} & -\dfrac{K_e}{L_{arm}} & 0 & 0 & 0 & 0 & 0 \\[2mm] \dfrac{K_t}{J_m} & -\dfrac{C_m}{J_m} & -\dfrac{n^2 K_m}{J_m} & 0 & \dfrac{n K_m}{J_m} & 0 & 0 \\[2mm] 0 & 1 & 0 & 0 & 0 & 0 & 0 \\[2mm] 0 & 0 & \dfrac{n K_m}{M_s} & -\dfrac{C_s}{M_s} & -\dfrac{K_s + K_m}{M_s} & \dfrac{C_s}{M_s} & \dfrac{K_s}{M_s} \\[2mm] 0 & 0 & 0 & 1 & 0 & 0 & 0 \\[2mm] 0 & 0 & 0 & \dfrac{C_s}{M_L} & \dfrac{K_s}{M_L} & -\dfrac{C_s}{M_L} & -\dfrac{K_s}{M_L} \\[2mm] 0 & 0 & 0 & 0 & 0 & 1 & 0 \end{bmatrix}, \quad B = \begin{bmatrix} \dfrac{1}{L_{arm}} \\[2mm] 0 \\[1mm] 0 \\[1mm] 0 \\[1mm] 0 \\[1mm] 0 \\[1mm] 0 \end{bmatrix} \quad (2.3)$$

$$C = \begin{bmatrix} 0 & 0 & 0 & 0 & 0 & 0 & 1 \end{bmatrix}$$

The meaning and value of the parameters and states are listed in Table 1. The motor parameters come from a real D.C. servo motor provided by McLennan Servo Supplies Ltd, Industrial DC Servo Motor M543E [12]. The other mechanical parameters are derived from [13].

TABLE 1

DEFINITION OF PARAMETERS AND STATES IN STATE SPACE MODEL

R_{arm}	motor resistance	2.2 Ω	L_{arm}	inductance of the windings	6.4 mH
K_e	voltage constant	0.121 V/rad/s	K_t	torque constant	0.121 Nm/A
J_m	motor inertia	5.3e-5 kgm^2	C_m	damping coefficient	8e-5 Nm/rad/s
K_m	motor stiffness	1e7 N/m	n	screw pitch	3.82e-4 m/rad
K_s	screw stiffness	1.8e5 N/m	C_s	Screw damping	1.2e3 N/m/s
M_s	screw mass	2 kg	M_L	load mass	20 kg
i_a	armature current	A	θ_m	angular rotation of the motor shaft	rad
X_m	screw position	m	X_L	end-of-actuator position	m

The actuator faults can be divided into two types: motor faults which occur in the D.C. motor as electrical faults, and the mechanical faults which happen in the components where the torque is

transferred to the load. The faults considered are summarised below.

2.2 Individual actuator faults

Overheating: This may either be caused by insulation breakdown leading to shorted turns, or to some field demagnetisation. In both cases it will cause reduction in the voltage constant K_e and the torque constant K_t .

Open circuit: The effect is that the resistance of the rotor will be very large so that almost no current will flow. Hence no torque will be generated by the motor.

Backlash: Generally, the backlash effect occurs due to wear in the screw/nut mechanism. Its effect can be described using a dead-zone [14].

Lockup: Excessive wear in the screw/nut mechanism may create mechanical interference within the mechanism such that the actuator becomes locked. This fault is serious as it can not be solved (by reconfiguration) at the signal level.

2.3 Modelling of two by two configuration

Having developed the basic (sub-actuator) model, it is relatively straightforward to build multi-actuator systems by combining the individual sub-actuators. There are two basic configurations to connect two individual actuators, one is in series and the other is in parallel. In the series configuration, one actuator is connected at the end of the other thereby doubling the extension length and velocity. In the parallel configuration, two actuators are connected to push/pull the same load so that the force output is doubled. Taking advantage of both these connecting structures, two separate actuators can be

developed and modelled. The first one is "parallel-in-series" (PS), as shown in the left of Fig. 6, and the

other one is denoted "series-in-parallel" (SP), as shown in the right of Fig. 6.

(a) parallel-in-series   (b) series-in-parallel
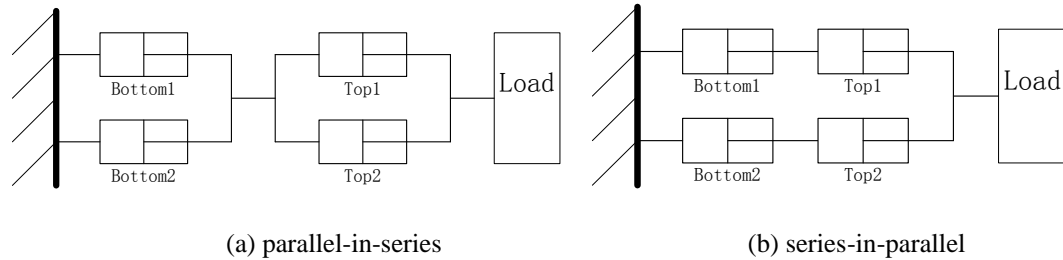
Fig. 6 Two kinds of two by two configurations

In a parallel structure, the elements are connected together at the end so that the structure will fail fixed

when one of them is locked up. The PS configuration comprises two parallel structures while the SP

only has one, so it will reduce the reliability under a lockup fault situation. For the present study the SP

configuration is adopted because of its greater reliability. The development of a model of the SP

configuration begins with the equivalent model of Fig 7 and the free body diagram shown in Fig 8.

Fig. 7 Equivalent model of two by two SP configuration

11

Fig. 8 Free body diagram of two by two SP configuration

In the SP configuration, the top actuator connected to the bottom actuator is seen as part of the load. In Fig 8, M_m represents the mass of the motor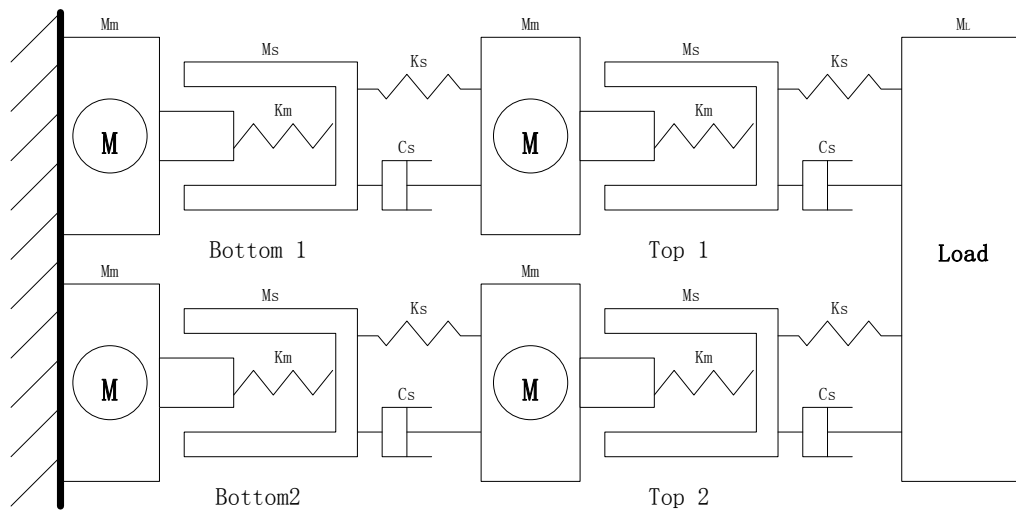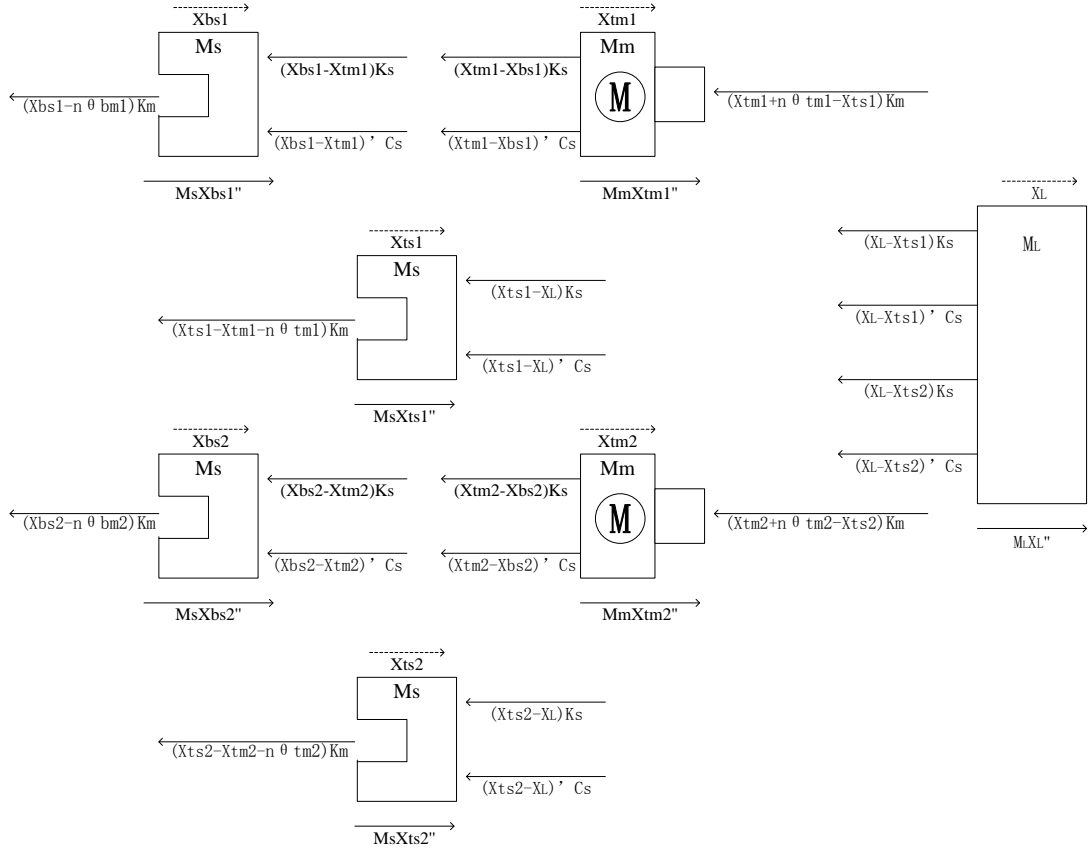; the subscript, b1 and b2 denote bottom actuator 1 and 2 respectively; t1 and t2 denote top actuator 1 and 2 as described in the equivalent model. According to the free body diagram, the following representation of the mechanical part can be obtained:

$$\begin{cases} M_s X''_{bs1} + \left(X_{bs1} - n\theta_{bm1}\right)K_m + \left(X_{bs1} - X_{tm1}\right)K_s + \left(X'_{bs1} - X'_{tm1}\right)C_s = 0 \\ M_m X''_{tm1} + \left(X_{tm1} - X_{bs1}\right)K_s + \left(X'_{tm1} - X'_{bs1}\right)C_s + \left(X_{tm1} + n\theta_{tm1} - X_{ts1}\right)K_m = 0 \\ M_s X''_{ts1} + \left(X_{ts1} - X_{tm1} - n\theta_{tm1}\right)K_m + \left(X_{ts1} - X_L\right)K_s + \left(X'_{ts1} - X'_L\right)C_s = 0 \\ M_s X''_{bs2} + \left(X_{bs2} - n\theta_{bm2}\right)K_m + \left(X_{bs2} - X_{tm2}\right)K_s + \left(X'_{bs2} - X'_{tm2}\right)C_s = 0 \qquad (2.4) \\ M_m X''_{tm2} + \left(X_{tm2} - X_{bs2}\right)K_s + \left(X'_{tm2} - X'_{bs2}\right)C_s + \left(X_{tm2} + n\theta_{tm2} - X_{ts2}\right)K_m = 0 \\ M_s X''_{ts2} + \left(X_{ts2} - X_{tm2} - n\theta_{tm2}\right)K_m + \left(X_{ts2} - X_L\right)K_s + \left(X'_{ts2} - X'_L\right)C_s = 0 \\ M_l X''_L + \left(X_L - X_{ts1}\right)K_s + \left(X'_L - X'_{ts1}\right)C_s + \left(X_L - X_{ts2}\right)K_s + \left(X'_L - X'_{ts2}\right)C_s = 0 \end{cases}$$

The equations for each of the four D.C. motors are identical to those for the individual actuator and it is assumed that all sub-actuation elements are driven from the same power supply. Assuming that all four actuators are identical, each actuator has the same parameter values as shown in Table 1. Combining equations 2.2 and 2.4 gives a twenty-six state state-space model with the input and output being the applied voltage and position of the load respectively.

In the structure of the SP configuration, state matrix A will comprise both the model of each individual sub-actuator and the coupling between the sub-actuators, thus it can be partitioned into a 4x4 matrix based on the physical meaning with elements b1, b2 (the bottom set of sub-actuators), t1, t2 (the top set of sub-actuators) in the diagonal, and their coupling relations in the off-diagonal positions.

$$
A = \begin{bmatrix}
b1 & b1*t1 & b1*b2 & b1*t2 \\
t1*b1 & t1 & t1*b2 & t1*t2 \\
b2*b1 & b2*t1 & b2 & b2*t2 \\
t2*b1 & t2*t1 & t2*b2 & t2
\end{bmatrix}_{4*4}
\quad \text{or,} \quad
A = \begin{bmatrix}
A_{11} & A_{12} & A_{13} & A_{14} \\
A_{21} & A_{22} & A_{23} & A_{24} \\
A_{31} & A_{32} & A_{33} & A_{34} \\
A_{41} & A_{42} & A_{43} & A_{44}
\end{bmatrix}_{4*4}
$$

In fact, the A_{ij} for all $i = 1,2,3,4$ and $j = 1,2,3,4$ sub-matrices are given as follows:

$$
A_{11} = \begin{bmatrix}
-\dfrac{R_{arm}}{L_{arm}} & -\dfrac{K_e}{L_{arm}} & 0 & 0 & 0 & 0 & 0 \\
\dfrac{K_t}{J_m} & -\dfrac{C_m}{J_m} & -\dfrac{n^2 K_m}{J_m} & 0 & \dfrac{n K_m}{J_m} & 0 & 0 \\
0 & 1 & 0 & 0 & 0 & 0 & 0 \\
0 & 0 & \dfrac{n K_m}{M_s} & -\dfrac{C_s}{M_s} & -\dfrac{K_s + K_m}{M_s} & \dfrac{C_s}{M_s} & \dfrac{K_s}{M_s} \\
0 & 0 & 0 & 1 & 0 & 0 & 0 \\
0 & 0 & 0 & \dfrac{C_s}{M_L} & \dfrac{K_s}{M_L} & -\dfrac{C_s}{M_L} & -\dfrac{K_m + K_s}{M_L} \\
0 & 0 & 0 & 0 & 0 & 1 & 0
\end{bmatrix}_{7*7},
\quad
A_{12} = \begin{bmatrix}
0 & 0 & 0 & 0 & 0 \\
0 & 0 & 0 & 0 & 0 \\
0 & 0 & 0 & 0 & 0 \\
0 & 0 & 0 & 0 & 0 \\
0 & 0 & 0 & 0 & 0 \\
0 & 0 & -\dfrac{n K_m}{M_m} & 0 & \dfrac{K_m}{M_m} \\
0 & 0 & 0 & 0 & 0
\end{bmatrix}_{7*5} ,
$$

$A_{13} = 0_{7*7}$, $A_{14} = 0_{7*7}$,

$$A_{21} = \begin{bmatrix} 0 & 0 & 0 & 0 & 0 & 0 & 0 \\ 0 & 0 & 0 & 0 & 0 & 0 & -\dfrac{nK_m}{J_m} \\ 0 & 0 & 0 & 0 & 0 & 0 & 0 \\ 0 & 0 & 0 & 0 & 0 & 0 & \dfrac{K_m}{M_s} \\ 0 & 0 & 0 & 0 & 0 & 0 & 0 \end{bmatrix}_{5*7}, \quad A_{22} = \begin{bmatrix} -\dfrac{R_{arm}}{L_{arm}} & -\dfrac{K_e}{L_{arm}} & 0 & 0 & 0 \\ \dfrac{K_t}{J_m} & -\dfrac{C_m}{J_m} & -\dfrac{n^2 K_m}{J_m} & 0 & \dfrac{nK_m}{J_m} \\ 0 & 1 & 0 & 0 & 0 \\ 0 & 0 & \dfrac{nK_m}{M_s} & -\dfrac{C_s}{M_s} & -\dfrac{K_m + K_s}{M_s} \\ 0 & 0 & 0 & 1 & 0 \end{bmatrix}_{5*5},$$

$$A_{23} = 0_{5*7}, \quad A_{24} = \begin{bmatrix} 0 & 0 & 0 & 0 & 0 & 0 & 0 \\ 0 & 0 & 0 & 0 & 0 & 0 & 0 \\ 0 & 0 & 0 & 0 & 0 & 0 & 0 \\ 0 & 0 & 0 & 0 & 0 & \dfrac{C_s}{M_s} & \dfrac{K_s}{M_s} \\ 0 & 0 & 0 & 0 & 0 & 0 & 0 \end{bmatrix}_{5*7},$$

$$A_{31} = 0_{7*7}, \quad A_{32} = 0_{7*5},$$

$$A_{33} = \begin{bmatrix} -\dfrac{R_{arm}}{L_{arm}} & -\dfrac{K_e}{L_{arm}} & 0 & 0 & 0 & 0 & 0 \\ \dfrac{K_t}{J_m} & -\dfrac{C_m}{J_m} & -\dfrac{n^2 K_m}{J_m} & 0 & \dfrac{nK_m}{J_m} & 0 & 0 \\ 0 & 1 & 0 & 0 & 0 & 0 & 0 \\ 0 & 0 & \dfrac{nK_m}{M_s} & -\dfrac{C_s}{M_s} & -\dfrac{K_s + K_m}{M_s} & \dfrac{C_s}{M_s} & \dfrac{K_s}{M_s} \\ 0 & 0 & 0 & 1 & 0 & 0 & 0 \\ 0 & 0 & 0 & \dfrac{C_s}{M_L} & \dfrac{K_s}{M_L} & -\dfrac{C_s}{M_L} & -\dfrac{K_m + K_s}{M_L} \\ 0 & 0 & 0 & 0 & 0 & 1 & 0 \end{bmatrix}_{7*7}, \quad A_{34} = \begin{bmatrix} 0 & 0 & 0 & 0 & 0 & 0 & 0 \\ 0 & 0 & 0 & 0 & 0 & 0 & 0 \\ 0 & 0 & 0 & 0 & 0 & 0 & 0 \\ 0 & 0 & 0 & 0 & 0 & 0 & 0 \\ 0 & 0 & 0 & 0 & 0 & 0 & 0 \\ 0 & 0 & -\dfrac{nK_m}{M_m} & 0 & -\dfrac{K_m}{M_m} & 0 & 0 \\ 0 & 0 & 0 & 0 & 0 & 0 & 0 \end{bmatrix}_{7*7},$$

$$A_{41} = 0_{7*7}, \quad A_{42} = \begin{bmatrix} 0 & 0 & 0 & 0 & 0 \\ 0 & 0 & 0 & 0 & 0 \\ 0 & 0 & 0 & 0 & 0 \\ 0 & 0 & 0 & 0 & 0 \\ 0 & 0 & 0 & 0 & 0 \\ 0 & 0 & 0 & \dfrac{C_s}{M_L} & \dfrac{K_s}{M_L} \\ 0 & 0 & 0 & 0 & 0 \end{bmatrix}_{7*5},$$

$$A_{43} = \begin{bmatrix} 0 & 0 & 0 & 0 & 0 & 0 & 0 \\ 0 & 0 & 0 & 0 & 0 & 0 & -\dfrac{nK_m}{J_m} \\ 0 & 0 & 0 & 0 & 0 & 0 & 0 \\ 0 & 0 & 0 & 0 & 0 & 0 & \dfrac{K_m}{M_s} \\ 0 & 0 & 0 & 0 & 0 & 0 & 0 \\ 0 & 0 & 0 & 0 & 0 & 0 & 0 \\ 0 & 0 & 0 & 0 & 0 & 0 & 0 \end{bmatrix}_{7*7}, \quad A_{44} = \begin{bmatrix} -\dfrac{R_{arm}}{L_{arm}} & -\dfrac{K_e}{L_{arm}} & 0 & 0 & 0 & 0 & 0 \\ \dfrac{K_t}{J_m} & -\dfrac{C_m}{J_m} & -\dfrac{n^2 K_m}{J_m} & 0 & \dfrac{nK_m}{J_m} & 0 & 0 \\ 0 & 1 & 0 & 0 & 0 & 0 & 0 \\ 0 & 0 & \dfrac{nK_m}{M_s} & -\dfrac{C_s}{M_s} & -\dfrac{K_s + K_m}{M_s} & \dfrac{C_s}{M_s} & \dfrac{K_s}{M_s} \\ 0 & 0 & 0 & 1 & 0 & 0 & 0 \\ 0 & 0 & 0 & \dfrac{C_s}{M_L} & \dfrac{K_s}{M_L} & -\dfrac{2C_s}{M_L} & -\dfrac{2K_s}{M_L} \\ 0 & 0 & 0 & 0 & 0 & 1 & 0 \end{bmatrix}_{7*7}$$

and the corresponding B,C matrices are:

$$B = \begin{bmatrix} \dfrac{1}{L_{arm}} & 0 & 0 & 0 & 0 & 0 & 0 & \dfrac{1}{L_{arm}} & 0 & 0 & 0 & 0 & \dfrac{1}{L_{arm}} & 0 & 0 & 0 & 0 & 0 & 0 & \dfrac{1}{L_{arm}} & 0 & 0 & 0 & 0 & 0 & 0 \end{bmatrix}^T,$$

$$C = \begin{bmatrix} 0 & 0 & 0 & 0 & 0 & 0 & 0 & 0 & 0 & 0 & 0 & 0 & 0 & 0 & 0 & 0 & 0 & 0 & 0 & 0 & 0 & 0 & 0 & 0 & 0 & 1 \end{bmatrix}$$
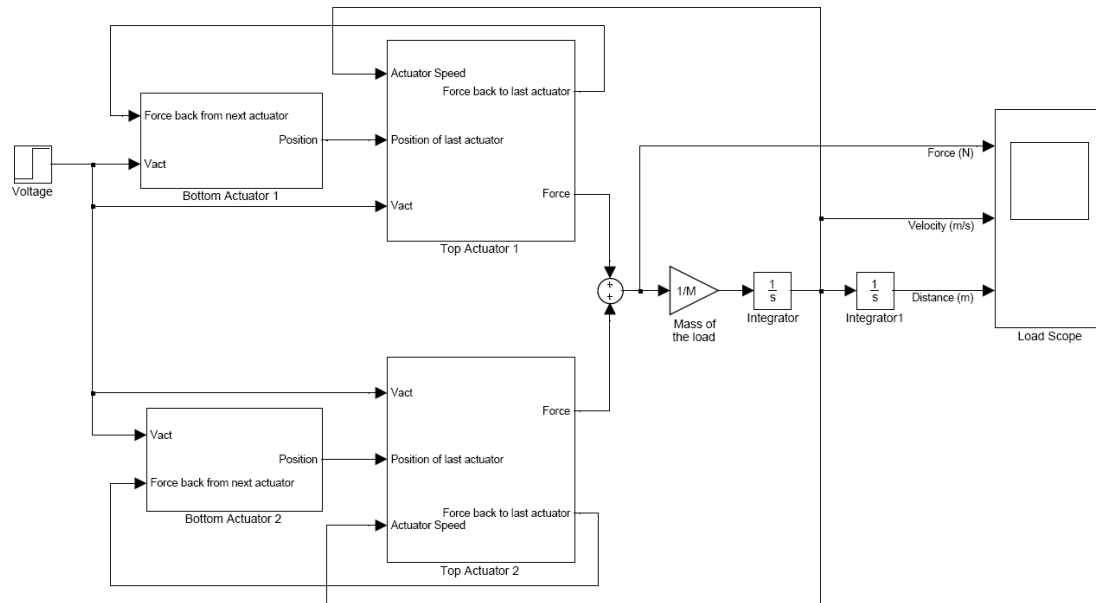
Fig. 9 Linear model of two by two SP configuration

A linear model built in MATLAB/Simulink is shown in Fig. 9. The coupling between the different actuators is clearly evident, by noting the interconnections of position and force information between the different actuators.

The aforementioned models can be used for control design and test of the closed-loop system under fault scenarios in Simulink.

3. Control Design

PID controllers as well as lead/lag compensator networks have been very successful classical control structures utilised in a number of industrial applications. It is rather straightforward to derive the required transfer function relationship needed for classical control design from the state space model. In particular, a position control design is followed, using two control schemes, i.e. a global controller

for the full actuator assembly and a global controller for the full actuator assembly with local

controllers at each sub-actuator, see Fig. 10.

(a) voltage-driven   (b) current-driven
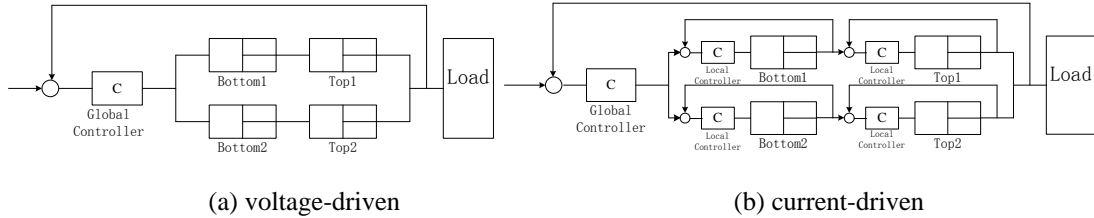
Fig. 10 Control structures

3.1 Control structure

Referring to Fig. 10 above, voltage-driven control comprises one controller based on the position

output of the HRA, while current-driven control is an extension including local controllers to regulate

the motor currents of each individual sub-actuator within the HRA.

Both control schemes use position feedback information for the global controller while Fig. 10(b) uses

additional current feedback information for the local controllers. The two control structures are

designed to provide similar performance thus enabling a fair comparison of the sensitivity to faults for

both structures (see section 4).

3.2 Controller design

First, the voltage-driven controller is considered. Since the open-loop system gain is very small at low

frequency (see Fig. 11), a proportional controller with a gain of 1000V/m is chosen for the global

position controller to raise the magnitude without overloading the D.C. motor. After the compensation, the phase margin (P.M.) is 83.7deg and the gain margin (G.M.) is 11.4dB so that no other compensator is needed. The closed-loop bandwidth is about 1Hz for the overall feedback system.
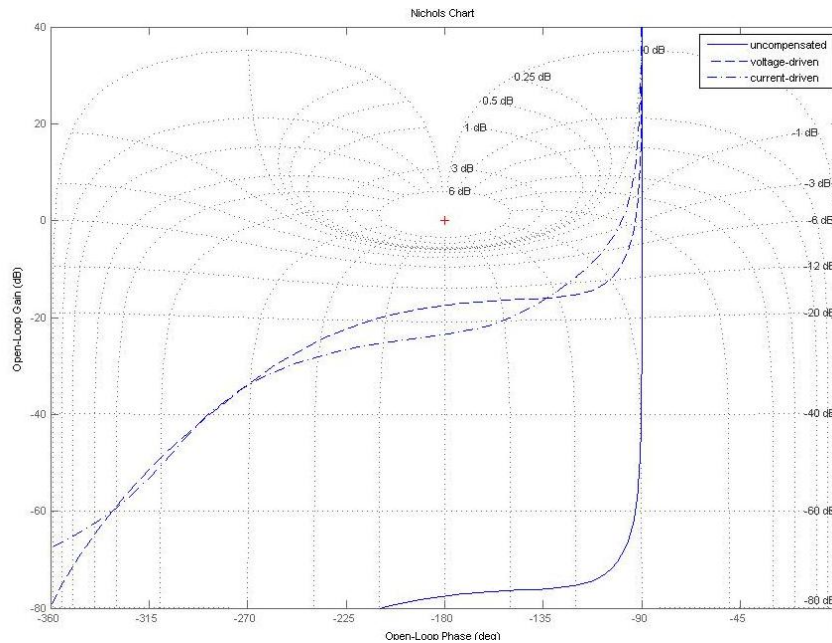
Fig. 11 Performance in frequency domain using classical control

For the structure with local current controller, generally a faster inner current loop is needed. Using integral controller with a gain of 800 V/A, the bandwidth of the current inner loop is set to about 75 Hz. Then a lead compensator is designed for the global position controller with a gain of 156.66 A/m, a zero of -1.09 and a pole of - 36.31. With this design, the P.M. is 80.8deg, the G.M. is 23.5dB, and the closed-loop bandwidth is again about 1Hz. A time domain response to a 0.06m step command is given in Fig. 12 for both control structure without and with local current control as well as the performance in frequency domain shown in an open loop Nichols chart for the uncompensated and compensated systems in Fig. 11.
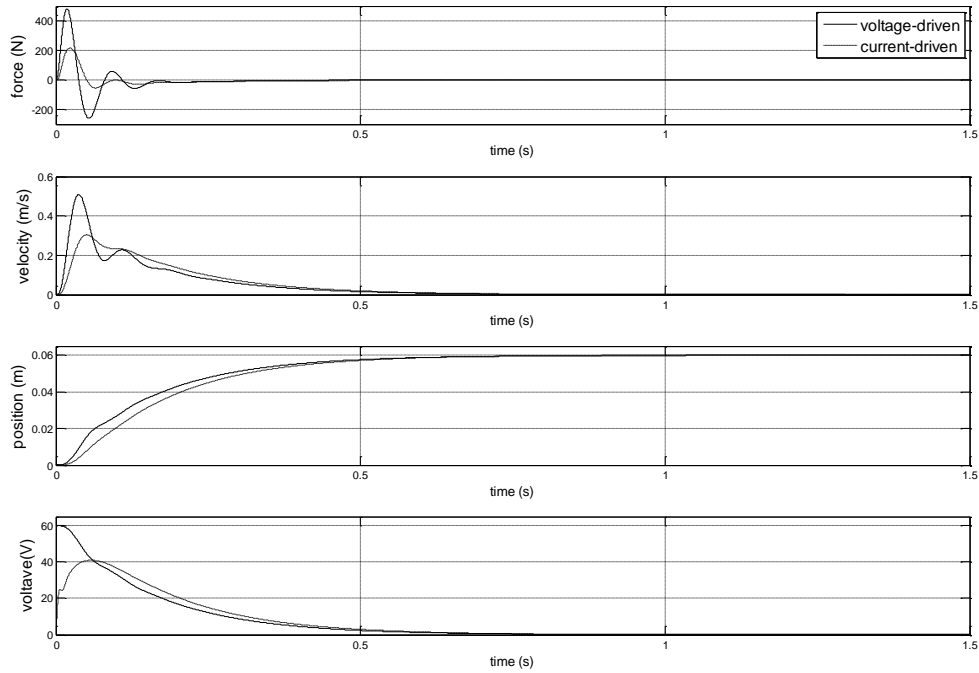
Fig. 12 Performance in time domain using classical control

Very similar performance can be seen for both voltage-driven and current-driven control structures because of the design process. But to get such similar performance, the output voltage of the current-driven controller is limited at 40V while the maxim output of voltage-driven controller is 60V, which means the system using current-driven structure can be faster than the one has been designed. The benefit of these systems having similar performance is that the behaviour of both schemes can be compared when faults are introduced.

4.   Simulation results

In sections 2 and 3, a two by two series-in-parallel configuration for a HRA has been modelled and controllers have been designed. In this section, the HRA is tested under fault-injected situations. Both the controller and the control structure remain unchanged when the fault is injected (i.e. there is no

reconfiguration).

Four kinds of actuator faults are modelled: Overheating, Open circuit, Backlash and Lockup. It should be noted that lock-up (fail-fixed) and open-circuit (fail-loose) are considered to be worst cases.

 The Bottom 1 sub-actuator, as shown in Fig. 6, is chosen as the fault injected element. Two kinds of control set-point input will be used for testing purpose, a step signal and a ramp signal. Both time and frequency domain performances will be compared to see how much degradation occurs in performance when faults are injected.   It should be noted that in the results below the actuator load is a moving mass, M, (see fig 7).   Application of other loads, such as applied external forces, was found to have very little effect on the overall results.

4.1 Step response

A 0.06m step signal will be used to test the step response of the SP configuration under both control structures. Fig. 13 shows the performance of the HRA using classical voltage-driven controller under healthy and locked up situations.   In the figure, the key parameter is the actuator position (third from top) which responds to a step in set-point from 0m to 0.06m at a time of 0seconds. It can be seen that the performance is slightly degraded (in terms of rise and settling times), but that the set-point is achieved even in the case of the locked fault. Other performances in both time and frequency domain (for this fault case and others) are summarised in Table 2.
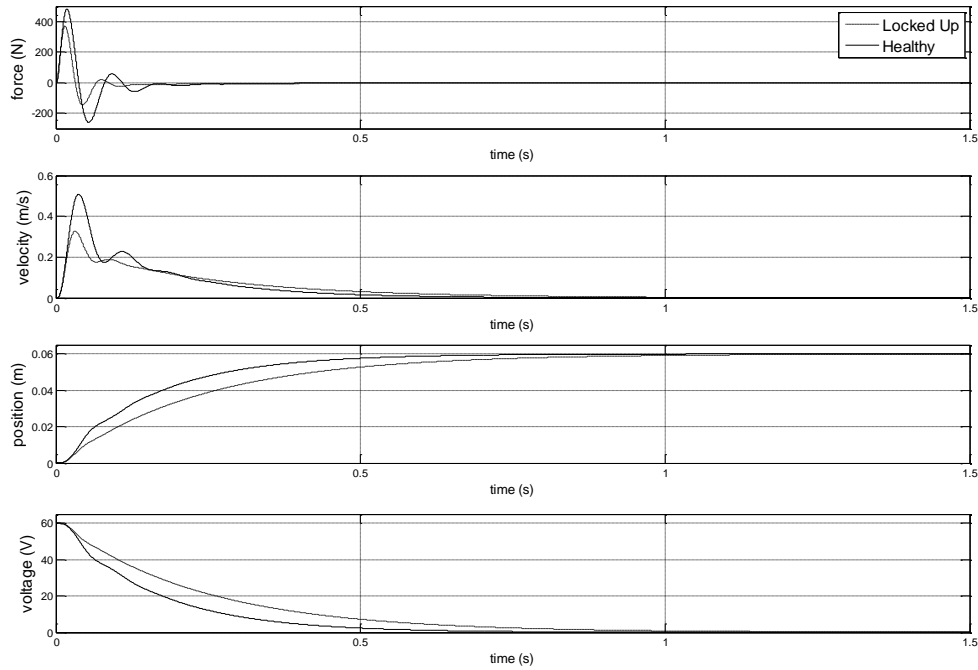
Fig. 13 Performance under healthy and locked up situation using voltage-driven controller

TABLE 2

Performance of SP configuration with voltage-driven (up) and current-driven (down) control structure

Performance Situations	FV(m)	RT(s)	ST(s)	OS	PM(deg)	GM(dB)	BW(Hz)
Voltage-driven							
Healthy	0.06	0.35	0.60	0%	83.7	11.4	1
Overheating	0.06	0.30	0.58	0%	85.1	18	1.33
Open circuit	0.06	0.36	0.61	0%	86.7	12.1	1
Backlash	0.06	0.35	0.60	0%	86.9	17.5	1
Lockup	0.06	0.54	0.91	0%	88	24.1	0.69
Current-driven							

Healthy	0.06	0.39	0.62	0%	80.8	23.5	1
Overheating	0.06	0.44	0.74	0%	82.1	24.4	0.88
Open circuit	0.06	0.40	0.62	0%	80.6	17.9	0.96
Backlash	0.06	0.40	0.62	0%	80.8	23.5	1
Lockup	0.06	0.60	0.99	0%	83.8	30.0	0.64

KEY: FV is Final value of position, RT is Rise time, ST is Settling time, and OT is overshoot, GM is Gain margin, PM is Phase margin, BW is Band width.

From the table listed above, firstly, the HRA can reach the reference position under all fault situationsand the degradation when faults are injected is not judged to be significant. For both controllers, the worst case is the lockup fault. With the level of redundancy being considered here, this kind of fault is more serious than the others because it can not be solved on a signal level. When this happens to an individual actuator, it only can be accommodated through redundancy rather than through a robust controller; hence degradation can be seen and expected.

For these two control structures, although performance degradation can be seen when faults are injected, it is hard to say which one is more sensitive to faults. It is possible to observe that there are bigger changes in bandwidth when faults occur in the voltage control case. However it's settling time is affected less than that of the current control. The changes in rise time are of a similar magnitude in both cases.

4.2 Ramp response

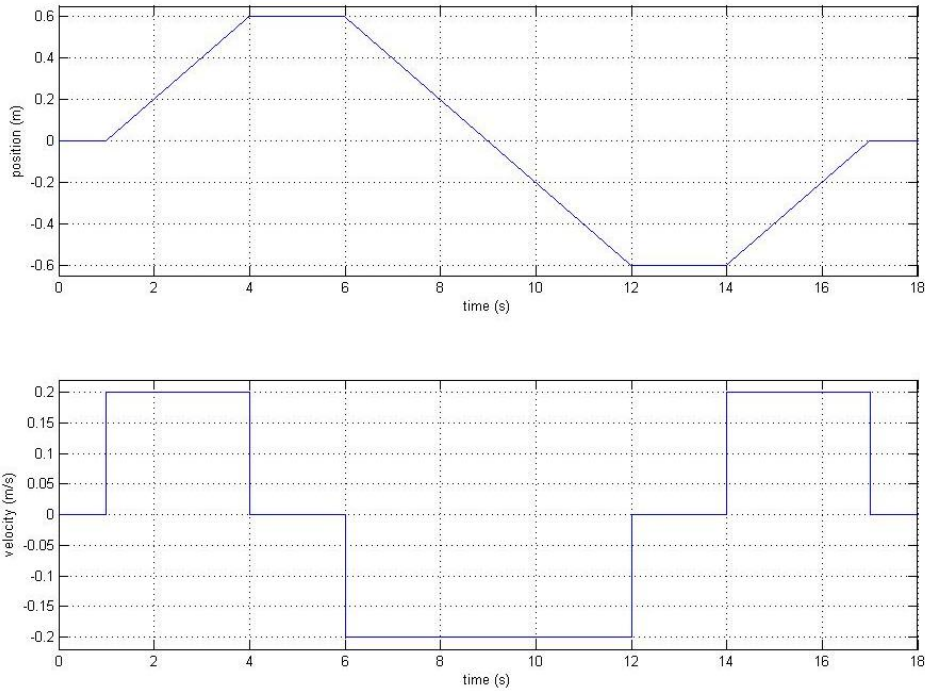
Fig. 14 Position and velocity input

A ramp position input is created between -0.6m and 0.6m with a slope of 0.2m/s. The velocity input is a step signal, while the position input is a ramp signal. The HRA uses the same controllers designed for the fault-free case via position feedback information. The command signal is shown in Fig. 14.
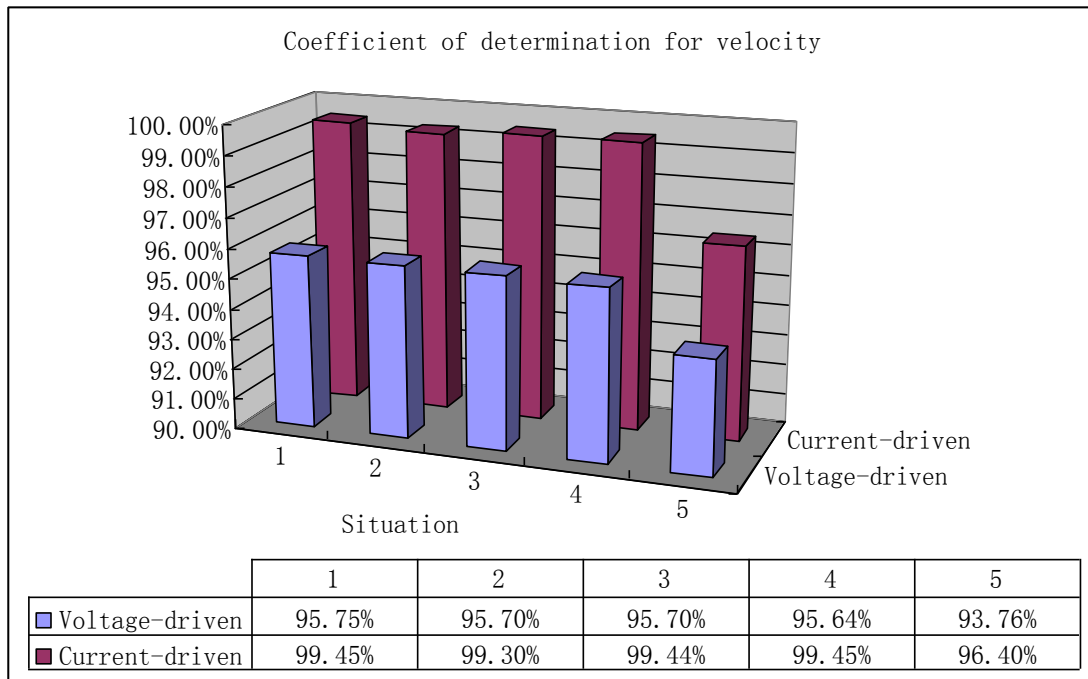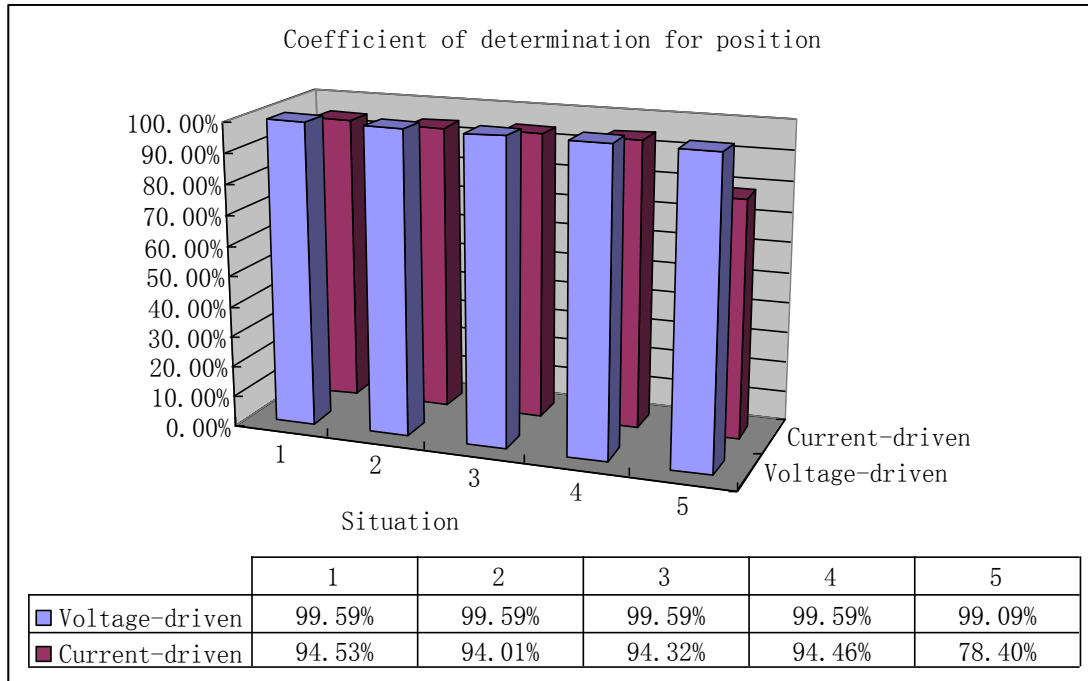
The coefficient of determination for both position and velocity output is calculated in each case. This is a statistical metric that measures how well the output tracks the input. It is given by the following equation:

$$rt^2 = 1 - \left(\frac{e}{y_d - mean(y_d)} \right)^2, \quad (4.1)$$

where e is the error between the input and output, y_d is the input value.

TABLE 3

Determination value for position and velocity of SP configuration with voltage-driven and

current-driven control structure

Coefficient of determination for position

	1	2	3	4	5
Voltage-driven	99.59%	99.59%	99.59%	99.59%	99.09%
Current-driven	94.53%	94.01%	94.32%	94.46%	78.40%

Coefficient of determination for velocity

	1	2	3	4	5
Voltage-driven	95.75%	95.70%	95.70%	95.64%	93.76%
Current-driven	99.45%	99.30%	99.44%	99.45%	96.40%

The results of determination values are listed in Table. 3 using two bar diagram to make it more visual.

23

Again, the Bottom 1 sub-actuator element is selected as the injected by faults. Five situations are listed. First is Healthy situation, and the others are Overheating, Open circuit, Backlash, and Lockup situations separately. Inspection of table 3 reveals that performance degradation can be found when faults are injected and the worst case is for the lockup fault, especially using current-driven control structure. The results also suggest that the voltage-driven structure is more suitable for position tracking while the current-driven structure is more suitable for velocity tracking (because a bigger value of determination coefficient for position is obtained in the voltage-driven structure while a bigger value of determination coefficient for velocity is found with the current-driven structure). The reason is due to the fast current inner loop added to the current-driven control structure. Since the current is a higher order state inside the HRA so that it makes the HRA easier to track a velocity or/and force command when current inner loops added. From this point of view, it can be concluded that the current-driven control structure is not as effective for position tracking purpose while the voltage-driven control structure can work on both position and velocity tracking purposes although a better performance can be obtained for a position tracking purpose.

5. Conclusion

The HRA is a novel actuator concept which provides the ability of fault tolerance without reconfiguration because it comprises a relatively large number of sub-actuation elements. This paper presented a linear model of a relatively simple two by two configuration of the HRA, as well as two candidate controllers designs based on a classical approach. The model has been set up and tested in MATLAB/Simulink. Four fault scenarios, including electrical and mechanical faults, were modelled to

test the fault tolerance ability of the HRA. The simulation results show some performance degradation occurs when faults are injected into one of the actuation elements, but the HRA can still complete the whole function without any reconfiguration at either mechanical or signal level. According to all these results, it's straightforward to conclude that the high redundancy actuator is relatively easy to control in both healthy and faulty situations. Both control structures proposed appear to be suitable for the task and there is little to choose between them.

For future work, extensions include testing the actuator with a large range of faults. More importantly the two by two configuration will be extended to four by four (and ultimately to higher dimensions), to ensure that the concept scales up. It should be noted that the models used in this study are linear, whilst actuators such as this do not generally exhibit high degrees of non-linearity, the effects of such issues and measurement noise have not been considered so far. To address this, an experimental HRA assembly based on the two by two SP configuration is currently being built together with the associated control system, which will help to confirm the practical viability of the HRA under both healthy and faulty situations. In the longer term it will also be important to consider possible applications for HRA and to investigate which design methods and actuation technologies are most appropriate for their manufacture.

6.   Acknowledgements

References

[1] R. Patton (1997). Fault Tolerant Control: The 1997 Situation. *SAFE-PROCESS'97, IFAC Symposium on fault detection, supervision and safety*, Kingston Upon Hull, U.K.

[2] D. Briere, C. Favre, and P. Traverse (1995). A family of Fault Tolerant Systems: Electrical flight controls from Airbus A320/A330/A340 to future military transport aircraft. *Microprocessors and Microsystems*, Volume 19, Number 2, pp. 75-82

[3] Terry. Ford (1998). Actuation systems development. *Aircraft Engineering and Aerospace Technology*, Volume 70, Number 4, pp. 265-270

[4] R. Isermann (1984). Process fault detection based on modelling and estimation methods – A survey. *Automatica*, Volume 20, No. 4, pp. 387-404

[5] R. Isermann, R. Schwarz, and S. Stolzl (2002). Fault-tolerant drive-by-wire systems. *IEEE Control Systems Magazine*, Volume 22, Issue 5, pp. 64 – 81

[6] G. Liu, and D. Wang (2004). Active fault tolerant control with actuation reconfiguration. *IEEE Transactions on Aerospace and Electronic Systems*, Vol. 40, No. 3 pp.1110 – 1117

[7] J. Lunze, and T. Steffen (2006). Control reconfiguration after actuator failures using disturbance decoupling methods. *IEEE Transactions on Automatic Control*, Vol. 51, No. 10, pp. 1590 – 1601

[8] H. Noura, D. Theilliol, and D. Sauter (2000). Actuator fault-tolerant control design: demonstration on a three-tank-system. *International Journal of Systems Science*, Vol. 31, No. 9, pp. 1143 – 1155

[9] G. Tao, S. M. Joshi, and X. Ma (2001). Adaptive state feedback and tracking control of systems with actuator failures. IEEE Transactions on Automatic Control, Vol. 46, No. 1, pp. 78 – 95

[10] W. Chen and J. Jiang (2005). Fault-tolerant control against stuck actuator faults. *IET* Control Theory & Applications, Vol. 152, No. 2, pp 138 – 146

[11] Y. Zhang, J. Jiang (2003). Fault tolerant control system design with explicit consideration of performance degradation. *IEEE Transactions on Aerospace and Electronic Systems*, Vol. 39, No. 3, pp. 838 - 848

[12] Mclennan Servo Supplies Ltd. http://www.mclennan.co.uk/

[13] Ian Pratt (1996). Active suspension applied to railway train, *PhD thesis in Loughborough University*, Section 1, pp. 59 – 66

[14] J. H. Baek, Y. K. Kwak, and S. H. Kim (2003). On the frequency bandwidth change of a servo system with a gear reducer due to backlash and motor input voltage. *Archive of Applied Mechanics*, Volume 73, pp. 367-376

[15] Ch. M. Hajiyev, and F. Caliskan (2001). Integrated sensor/actuator FDI and reconfigurabl3 control for fault-tolerant flight control system design, *The Aeronautical Journal (2001)*, pp. 525 - 533

[16] Slotine, J.E., Li, W. (1991). Applied nonlinear control. USA, Prentice-Hall

[17] X. Du, R. Dixon, R. M. Goodall, and A. C. Zolotas (2006). Assessment of strategies for control of high redundancy actuators, *Proceedings of the ACTUATOR 2006*, Bremen, Germany

[18] X. Du, R. Dixon, R. M. Goodall, and A. C. Zolotas (2006). Modelling and control of a highly redundant actuator, *International Control Conference 2006*, Glasgow, U.K.

List of Figures

List of Tables